



CrossMark  
 click for updates

Cite this: *RSC Adv.*, 2017, 7, 7763

## Formation mechanism of hafnium oxide nanoparticles by a hydrothermal route

Yingying Wan and Xingping Zhou\*

Hafnium oxide nanoparticles (NPs) were synthesized by a hydrothermal route, using hafnium tetrachloride ( $\text{HfCl}_4$ ) as the starting material and sodium hydroxide (NaOH) to adjust the pH. Through changing the aging temperature, concentration of NaOH and reaction time, both pure tetragonal hafnium oxide (t- $\text{HfO}_2$ ) and pure monoclinic hafnium oxide (m- $\text{HfO}_2$ ) were obtained. X-ray diffraction (XRD) spectra and transmission electron microscopy (TEM) images indicated that the shapes of t- $\text{HfO}_2$  NPs and m- $\text{HfO}_2$  NPs were near-spherical and spindle-like, respectively. The formation of t- $\text{HfO}_2$  NPs or m- $\text{HfO}_2$  NPs is probably related to their crystal cell structure, thermodynamic and kinetic stabilities. Tetragonal  $\text{HfO}_2$  is produced originally in the process of the formation of monoclinic  $\text{HfO}_2$ . A higher temperature, lower concentration of NaOH, longer reaction time and addition of m- $\text{HfO}_2$  seeds are beneficial for the formation of m- $\text{HfO}_2$  NPs. By analysis and calculation of the equilibrium constants involving hydrolysis of hafnium ions, the changes in the mole fractions of hafnium hydro-complexes with pH were determined. The  $\text{Hf}(\text{OH})_6^{2-}$  ion is assigned to the precursory hydro-complex for the formation of  $\text{HfO}_2$  nanoparticles transformed from  $\text{Hf}(\text{OH})_4$  gel according to a comparison between the influences of pH on the equilibrium and the formation of  $\text{HfO}_2$  particles. Moreover, the formation of  $\text{HfO}_2$  NPs was obviously promoted and the size was reduced by addition of seeds, suggesting that the formation of  $\text{HfO}_2$  NPs is controlled by the surface-deposition reaction. The above results are of great importance for studying nano-inorganic solution chemistry.

Received 11th November 2016  
 Accepted 17th January 2017

DOI: 10.1039/c6ra26663k

[www.rsc.org/advances](http://www.rsc.org/advances)

## Introduction

Nanostructured materials have a lot of important applications in various fields because of their unique properties.<sup>1–3</sup> Hafnium is known as the “little brother” of titanium and zirconium. Its dioxide ( $\text{HfO}_2$ ) is a material with a number of technologically attractive properties such as high melting point (2758 °C), high dielectric constant ( $\approx 30$ ), high chemical stability, a wide band gap ( $>5.0$  eV), and high neutron absorption cross section.<sup>4,5</sup> It often plays an important role in the continuous down-scaling of integrated circuits since new insulating materials with a high dielectric constant are being researched to replace  $\text{SiO}_2$  as a gate dielectric.<sup>6,7</sup> In terms of structural characteristics, hafnium oxide exists in three polymorphic structures, namely monoclinic (m- $\text{HfO}_2$ ) at low temperature, tetragonal (t- $\text{HfO}_2$ ) above 2050 K, and cubic (c- $\text{HfO}_2$ ) at around 2803 K.<sup>8–10</sup> Each structure has different applications.

The optical, electrical and other properties of  $\text{HfO}_2$  nanoparticles (NPs) are strongly affected by their size, morphology, and surface characteristics.<sup>11,12</sup> Therefore, it is necessary to consider the required specifications of  $\text{HfO}_2$  NPs before

choosing the synthesis method. Up to now, researchers have developed some synthesis approaches such as gel-sol method,<sup>13</sup> microemulsion processes<sup>14</sup> and precipitation.<sup>10,15</sup> However, these methods have some drawbacks, such as complicated operation, low yield and agglomerated products. In addition, all these ways only can obtain the m- $\text{HfO}_2$  NPs. Preparation of t- $\text{HfO}_2$  NPs has been rarely reported so far. More importantly, the formation mechanism and crystal form or morphology control of  $\text{HfO}_2$  NPs are less reported.

Recently, many efforts have been undertaken to improve the synthesis method. As a promising approach, hydrothermal synthesis<sup>16–18</sup> is widely used to synthesize nanocrystalline oxide materials due to the mild reaction condition, simple operation and no roasting. A. Sahraneshin<sup>16</sup> synthesized three differently shaped  $\text{HfO}_2$  NPs *via* a surfactant-assisted hydrothermal reaction in highly alkaline media. The products obtained were flower-like nanostructures (20.0 nm in diameter), polycrystalline nanoagglomerates (25.0 nm in diameter), and water-dispersible single nanoparticles (4.0 nm in diameter). In addition, S. A. Eliziario<sup>8</sup> successfully obtained the  $\text{HfO}_2$  NPs by the microwave hydrothermal method. The temperature chosen was 140 °C and these nanostructures exhibited an average width in the range from 15.0 to 75.0 nm as well as an average height between 85.0 and 105.0 nm. The hydrothermal method allows to control size, morphology and the composition of the

College of Chemistry, Chemical Engineering and Biotechnology, Donghua University, Shanghai 201620, PR China. E-mail: [xpzhou@dhu.edu.cn](mailto:xpzhou@dhu.edu.cn); Fax: +86-21-67792657; Tel: +86-21-67792657



products, and to obtain homogeneous and dispersed nanoparticles, through varying parameters such as temperature, pressure, duration of the process, concentration and acidity (pH).<sup>19–21</sup> The control of particle size and morphology is the result of processes of coarsening and redissolution–recrystallization which takes place under conditions of high pressure and temperature. The main advantages of hydrothermal method are simplicity and convenience.

In common, hydrothermal method still needs improvement in terms of yield, monodispersity, structural perfection, and size control. For synthesizing some nanoparticles, seeding is a very effective way to control particle size, to determine the crystal form<sup>22</sup> and even to study the nucleation and growth mechanisms. Some researchers have made in-depth studies on this technology. Our previous studies reported that the addition of seeds has been able to systematically control the particle morphology and studied the nucleation and growth mechanisms of ZrO<sub>2</sub> (ref. 22) and TiO<sub>2</sub>.<sup>23</sup> The seeds inhibit aggregation and the formation of secondary particles, so as to obtain the product wanted. Generally, the surface-deposition of monomers is not often the rate-determining step for the formation of nanoparticles unless the formation is accelerated and the particle size is controlled by seeding. Also, in this case, the size-distribution of nanoparticles is commonly narrowed.

In this paper, we used a hydrothermal route to prepare hafnium oxide nanoparticles. Effects of temperature, NaOH concentration, duration and crystal form of seeds were investigated to study the formation mechanisms of HfO<sub>2</sub> NPs from aspects of precursory complexes, thermodynamic and kinetic stabilities.

## Experimental

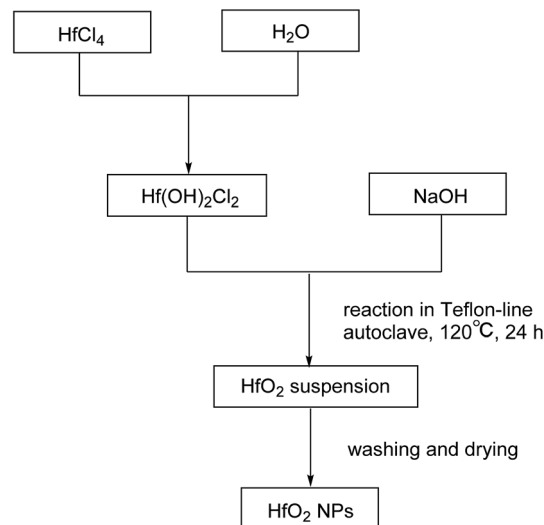
### Materials

HfCl<sub>4</sub> (AR, 99.0%), sodium hydroxide (AR, 96.0%), sodium dodecyl-benzenesulfonate (AR, 88.0%), dodecylamine (CP) were all purchased from Sinopharm Chemical Reagent Co., Ltd.

### Synthesis

**Preparation of HfO<sub>2</sub> nanoparticles.** The HfO<sub>2</sub> nanoparticles (NPs) were synthesized by the hydrothermal route. The standard experimental procedure is described as follows. The hafnium hydroxide chloride (Hf(OH)<sub>2</sub>Cl<sub>2</sub>) solution was firstly prepared by dissolving 0.160 g of HfCl<sub>4</sub> in 10.0 mL of de-ionized water. NaOH aqueous solution (3.0 M, 10.0 mL) was added dropwise to the solution above, causing the reaction with Hf(OH)<sub>2</sub>Cl<sub>2</sub> to form hafnium hydroxide (Hf(OH)<sub>4</sub>). After that, the solution was transferred into a 100 mL Teflon-lined autoclave with inner diameter of ca. 4.2 cm, and the sealed autoclave was heated to 120 °C and maintained for 24 h. The products were purified by centrifugation for three cycles with alcohol and de-ionized water alternately after the autoclave was cooled down. Finally the precipitate was dried at 50 °C for 24 h. The procedure is summarized in Scheme 1.

**Preparation of tetragonal and monoclinic HfO<sub>2</sub> seeds.** The synthesis procedure of monoclinic HfO<sub>2</sub> (m-HfO<sub>2</sub>) seeds is



Scheme 1 Preparation of HfO<sub>2</sub> NPs.

described as follows. To the solution prepared by dissolving 0.160 g of HfCl<sub>4</sub> in 8.0 mL of de-ionized water, 10.0 mL NaOH was added in order to make 0.1 M NaOH in aqueous phase, and 2.0 mL of 0.1 M dodecylamine solution was mixed with the solution above by stirring for 2–3 h. Hereafter, the resulting mixture was transferred into a 100 mL Teflon-lined autoclave with inner diameter of ca. 4.2 cm and maintained for 24 h after heated to 160 °C. On the other hand, to obtain tetragonal HfO<sub>2</sub> (t-HfO<sub>2</sub>) seeds, 5.0 mL of de-ionized water including 0.160 g of HfCl<sub>4</sub> was added to 10 mL of 0.1 M sodium dodecyl-benzenesulfonate solution, along with agitation of 2–3 h. Then the mixture was transferred into a 100 mL Teflon-lined autoclave with addition of 5.0 mL NaOH solution to make 3.0 M NaOH in aqueous phase. Afterwards, the autoclave was sealed and maintained for 24 h after heated to 100 °C.

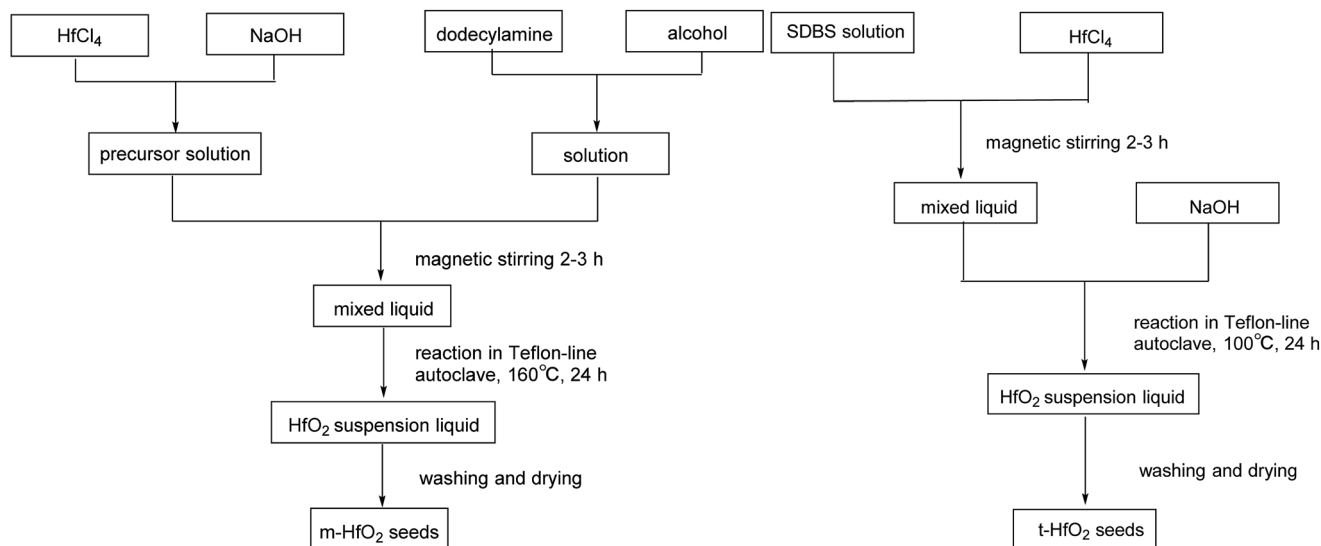
The products were purified by centrifugation for three cycles with alcohol and de-ionized water alternately after the autoclave was cooled down. Finally the precipitate was dried at 50 °C for 24 h. The procedures are summarized in Scheme 2.

## Characterization

The different morphologies and phases presenting in the solids were measured using X-ray powder diffraction (XRD, D/max, Rigaku, Tokyo, Japan) with Cu-K $\alpha$  radiation ( $\lambda = 1.5418 \text{ \AA}$ ) in a  $2\theta$ - $\theta$  setup, the  $2\theta$  angle was scanned from 0 to 90°. JADE software (MDI JADE 7 Materials Data XRD Pattern Processing, Identification, and Quantification) was used to evaluate/analyze the XRD patterns. The JCPDS card no. 06-0318 and the JCPDS card no. 53-0550 were used as the XRD standard files of m-HfO<sub>2</sub> and t-HfO<sub>2</sub>, respectively. The pH was measured by Sartorius PB-10.

Transmission electron microscopy (TEM) images were recorded with a JEOL JEM 2100F transmission electron-microscope, to analyze the product size and morphology. The samples used for TEM observations were prepared by dispersing the NPs in ethanol followed by ultrasonic vibration



Scheme 2 Preparation of HfO<sub>2</sub> seeds.

for 30 min, and then placing a drop of this dispersion onto a copper grid before loading into the instrument.

## Results and discussion

### Preparation of HfO<sub>2</sub>

Fig. 1 shows the XRD spectra of both tetragonal hafnium oxide nanoparticles (t-HfO<sub>2</sub> NPs) and monoclinic hafnium oxide nanoparticles (m-HfO<sub>2</sub> NPs) prepared. The tetragonal phase of HfO<sub>2</sub> was obtained under otherwise the standard conditions at 100 °C, the monoclinic phase of HfO<sub>2</sub> was obtained at 160 °C. In Fig. 1(a), the major characteristics peaks found at 30.48°, 35.30°, 50.68°, 60.26° on the  $2\theta$  scale correspond to the {111}, {200}, {220} and {311} planes respectively, in good agreements

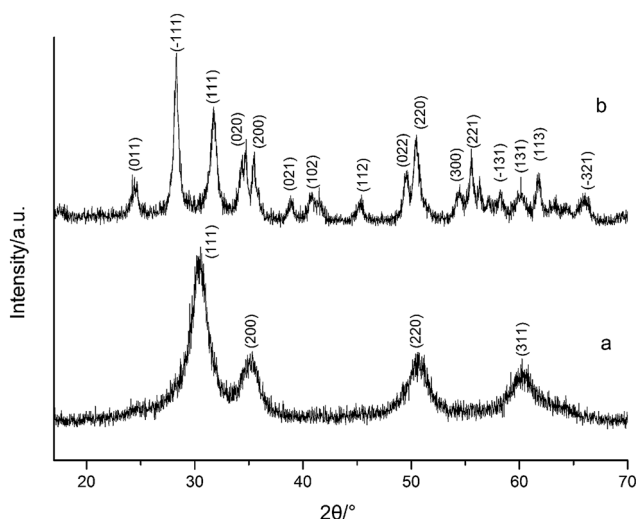


Fig. 1 XRD spectra of HfO<sub>2</sub> NPs prepared under otherwise the standard conditions (3.0 M NaOH and 24 h) at different temperatures: (a) 100 °C, (b) 160 °C.

with the standard PDF card of t-HfO<sub>2</sub> (JCPDS: no. 53-0550). The corresponding TEM image of near-spherical t-HfO<sub>2</sub> particles (4.0 nm) is presented in Fig. 2(a). In Fig. 1(b), the major characteristics peaks found at 24.64°, 28.30°, 31.76°, 50.46° on the  $2\theta$  scale correspond to the {011}, {-111}, {111}, {220} planes respectively, in good agreements with the standard PDF card of m-HfO<sub>2</sub> (JCPDS: no. 06-0318). The corresponding TEM images of spindle-like m-HfO<sub>2</sub> particles (*ca.* 100 nm × 50 nm) with a high aspect ratio is presented in Fig. 2(b). These nanoparticles are uniform, but some particles gather together.

The high-resolution TEM images shown in Fig. 2(a1) indicates high crystallinity of the structure, the  $d$  spacing of lattice fringes of 0.25 nm and 0.29 nm are indexed to the (200) and (111) plane of t-HfO<sub>2</sub>, respectively. In Fig. 2(b1), the  $d$  spacing of lattice fringes of 0.28 nm and 0.32 nm are indexed to the (111) and (-111) plane of m-HfO<sub>2</sub>, respectively. All the  $d$  spacing values are in close agreement with those from t-HfO<sub>2</sub> (JCPDS: no. 53-0550) and m-HfO<sub>2</sub> (JCPDS: no. 06-0318).

### Effects of reaction conditions on the formation of HfO<sub>2</sub> nanoparticles

**Reaction time.** Fig. 3 and 4 present XRD spectra and TEM images of the products obtained with different aging time at 120 °C under the otherwise conditions. After aging for 3 h, fine near-spherical particles of 4 nm in diameter were found in Fig. 4(a) and proved to be tetragonal phase by the XRD spectrum in Fig. 3. Shown as the white circle in Fig. 4(a), the particles grew and aggregated with the time going and the spindle-like particles began to appear after aging for 24 h, as displayed in Fig. 4(b) in the white circle. Virtually, at this time the product has been a mixture of t-HfO<sub>2</sub> and m-HfO<sub>2</sub> NPs, as exhibited in the XRD spectrum in Fig. 3. After aging for 72 h, from XRD spectrum in Fig. 3, the nanoparticles have been transformed into spindle-like m-HfO<sub>2</sub> (*ca.* 120 nm × 52 nm) completely, as also being confirmed by that in Fig. 4(c).



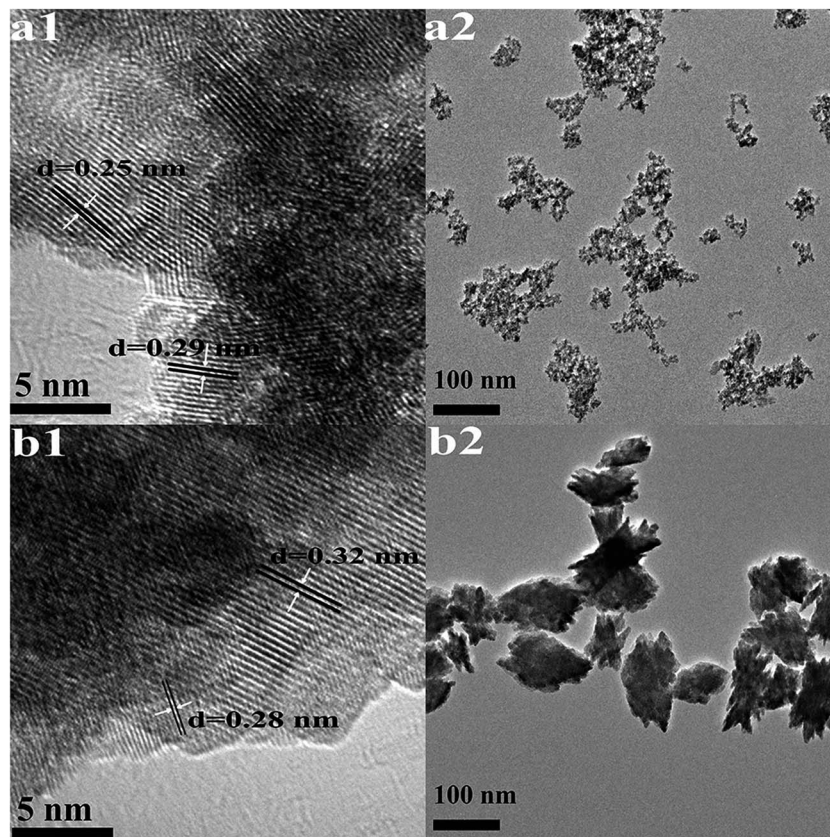


Fig. 2 HRTEM images (1) and TEM images (2) of HfO<sub>2</sub> NPs prepared under otherwise the standard conditions (3.0 M NaOH and 24 h) at different temperatures: (a) 100 °C, (b) 160 °C.

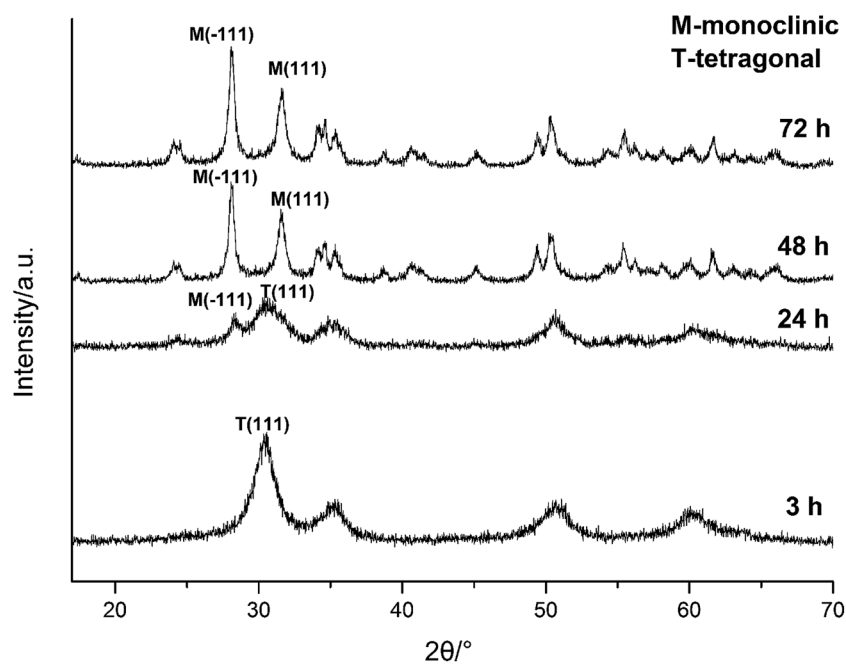


Fig. 3 XRD spectra of HfO<sub>2</sub> NPs prepared under otherwise the standard conditions (3.0 M NaOH and 120 °C) with different reaction time.



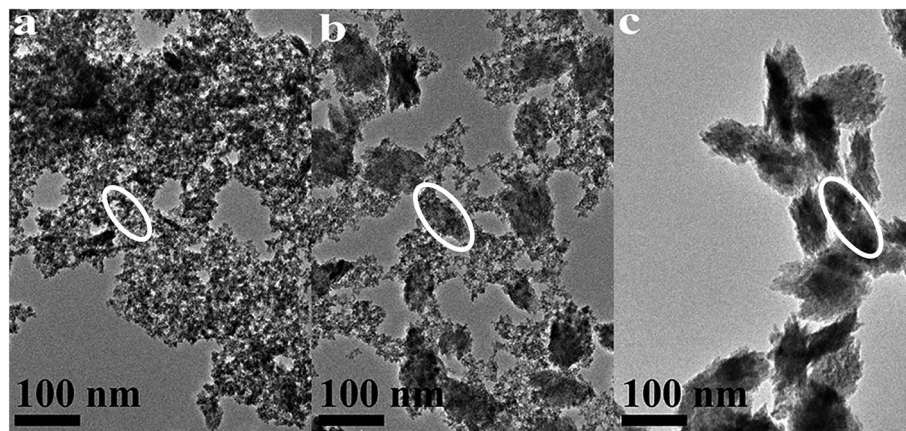


Fig. 4 TEM images of  $\text{HfO}_2$  NPs prepared under otherwise the standard conditions (3.0 M NaOH and 120 °C) with different reaction time: (a) 3 h, (b) 24 h, (c) 72 h.

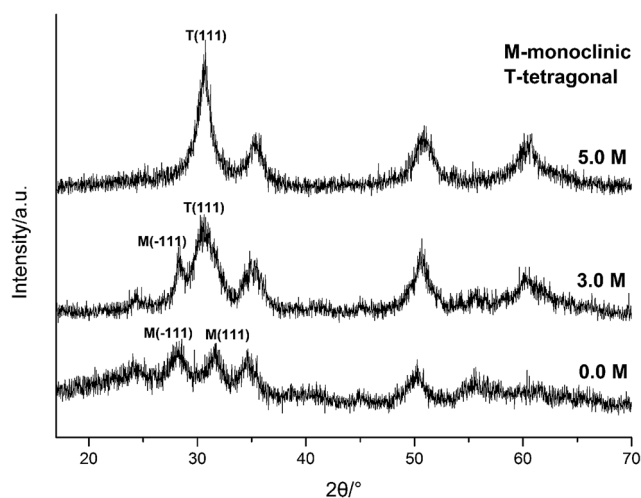


Fig. 5 XRD spectra of  $\text{HfO}_2$  NPs prepared under otherwise the standard conditions (120 °C and 24 h) with different concentrations of NaOH.

The above analysis reflected a phenomenon that the m- $\text{HfO}_2$  was not formed at beginning, but transformed from the t- $\text{HfO}_2$ . In the early stage of reaction, the t- $\text{HfO}_2$  NPs were firstly generated and then aggregated to form large secondary particles, which subsequently re-crystallized to produce m- $\text{HfO}_2$  NPs. This fact indicates that m- $\text{HfO}_2$  NPs probably have lower kinetic stability and higher thermodynamic stability in comparison to t- $\text{HfO}_2$  NPs.

**Concentration of NaOH.** XRD spectra in Fig. 5 show the diffraction peaks associated with m- $\text{HfO}_2$  and t- $\text{HfO}_2$  forms at different concentrations of NaOH. The main peaks of t- $\text{HfO}_2$  appeared in the presence of 5.0 M NaOH (pH = 14.0), the corresponding TEM image of near-spherical  $\text{HfO}_2$  particles (3.0 nm) is presented in Fig. 6(a). It was clearly observed that with decreasing concentration of NaOH to 3.0 M (pH = 12.5), the low peaks in Fig. 5 and the spindle-like particles in Fig. 6(b) indicated the generation of m- $\text{HfO}_2$ . Further decreasing led to the decline of peaks of t- $\text{HfO}_2$  and the enhancement of the peaks of m- $\text{HfO}_2$  in Fig. 5. Meantime, from Fig. 6(b), the mixture of the near-spherical and spindle-like  $\text{HfO}_2$  particles was found.

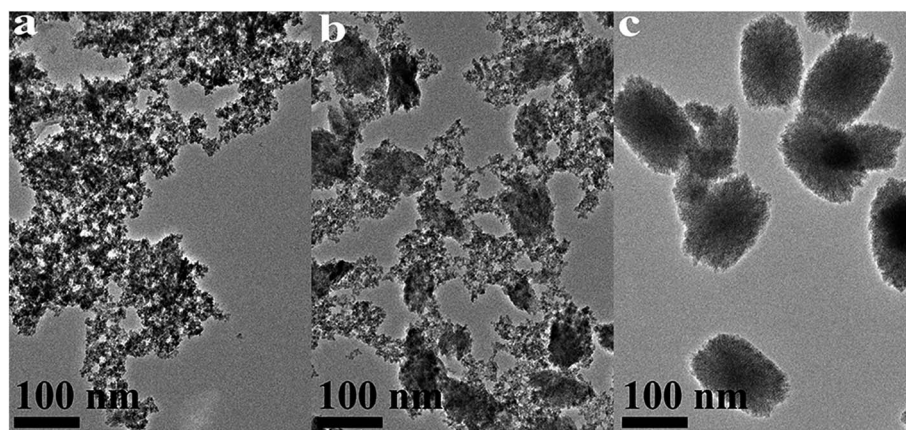


Fig. 6 TEM images of  $\text{HfO}_2$  NPs prepared under otherwise the standard conditions (120 °C and 24 h) with different concentrations of NaOH: (a) 5.0 M, (b) 3.0 M, (c) 0 M.



Decreasing NaOH concentration from 5.0 M to 0 resulted in the formation of m-HfO<sub>2</sub> (ca. 115 nm × 70 nm), indicated in Fig. 6(c).

Carefully considering the influence of pH or alkaline concentration on the formation of metal oxide from metal hydroxide, some metal hydro-complexes usually play a key role to the formation of metal oxide like TiO<sub>2</sub> (ref. 24 and 25) and ZrO<sub>2</sub>.<sup>22,26</sup> Jia *et al.*<sup>27</sup> suggested that the pH of the reaction mixture can control the dissociation rate of the precursor, which significantly affects the supply of metal ions or metal hydro-complexes in the reaction environment and thus the growth rate of the metal-oxide nanocrystals. For HfO<sub>2</sub> particles, precursory complex Hf(OH)<sub>x</sub><sup>4-x</sup> (x ≥ 5), has been suggested<sup>28</sup> from its influence on the particle size. On the other hand, A. Sahraneshin<sup>16</sup> proposed that the concentration of alkali can affect the growth of (111) plane of HfO<sub>2</sub> which was unstable with higher surface energy. For the current synthesis of HfO<sub>2</sub>, with no doubt, the high concentration of NaOH is of benefit to the

formation of primary t-HfO<sub>2</sub> NPs, this may be related to the effects of NaOH concentration on the precursor complex, which will be discussed in details in the latter section.

**Reaction temperature.** Undoubtedly, temperature is a key factor for the control of crystal forms. From the XRD spectra displayed in Fig. 7, the tetragonal phase of HfO<sub>2</sub> (4.0 nm) obtained at 100 °C under otherwise the standard conditions, the corresponding TEM image of near-spherical t-HfO<sub>2</sub> particles is presented in Fig. 8(a). The main peaks of t-HfO<sub>2</sub> became more obvious and the near-spherical particles began to accumulate as the temperature rose. Hereafter, the weak peak of M (-111) of m-HfO<sub>2</sub> appeared at 120 °C indicated the trend of formation of m-HfO<sub>2</sub> as also revealed from that some tiny embryos of spindle-like m-HfO<sub>2</sub> NPs were discernible in Fig. 8(b). Indeed, all the nanocrystals were fully transformed into monoclinic phase in the temperature range of 140–160 °C. The well crystallized monoclinic phase of HfO<sub>2</sub> was obtained under the standard conditions at 160 °C, the corresponding TEM image of spindle-like m-HfO<sub>2</sub> particles (ca. 100 nm × 50 nm) is presented in Fig. 8(c).

Based on the XRD and TEM observation in Fig. 7 and 8, the reaction temperature is also the key factor that influences particle morphology under the fixed alkaline concentration and reaction time. It has been reported that with the increase of temperature, the particles are more likely to collide to form a large particle even with different form at enough high temperature.<sup>23–25</sup> In this work, t-HfO<sub>2</sub> NPs may collide mutually and transform to m-HfO<sub>2</sub> NPs with the increase of temperature. Therefore, higher temperature, lower concentration of NaOH, and longer reaction time are beneficial for the formation of monoclinic hafnium oxide nanoparticles.

**Seeding.** Fig. 9 exhibits XRD spectra of HfO<sub>2</sub> nanocrystals prepared at 120 °C for 24 h with 3.0 M NaOH in the presence and the absence of HfO<sub>2</sub> seeds. It was found that without seeds, both the main peaks of m-HfO<sub>2</sub> and t-HfO<sub>2</sub> appeared simultaneously, indicating that the product was a mixture of t-HfO<sub>2</sub> and m-HfO<sub>2</sub> particles, but in the presence of t-HfO<sub>2</sub> seeds, the main peaks were associated with t-HfO<sub>2</sub>. Due to the addition of

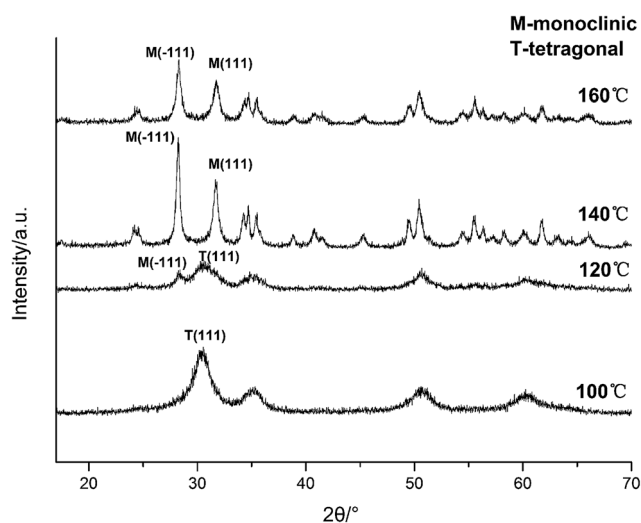


Fig. 7 XRD spectra of HfO<sub>2</sub> NPs prepared under otherwise the standard conditions (3.0 M NaOH and 24 h) at different temperatures.

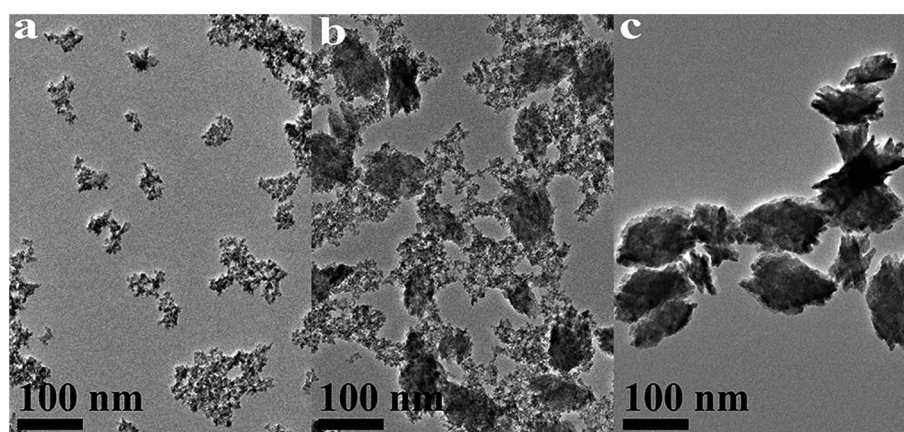


Fig. 8 TEM images of HfO<sub>2</sub> NPs prepared under otherwise the standard conditions (3.0 M NaOH and 24 h) at different temperatures: (a) 100 °C, (b) 120 °C, (c) 160 °C.



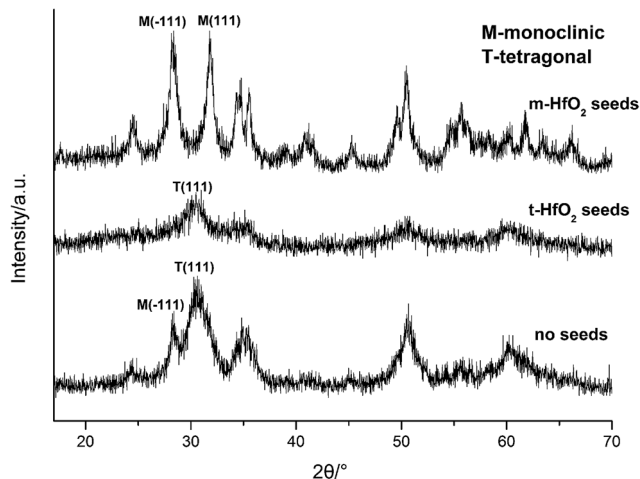


Fig. 9 XRD spectra of HfO<sub>2</sub> NPs prepared with different seeds.

tetragonal seeds, the solute monomers deposited on the pre-existing t-HfO<sub>2</sub> seeds and the size of the formed t-HfO<sub>2</sub> NPs became larger and larger, inhibiting aggregation and the formation of secondary particles, and preventing the production of m-HfO<sub>2</sub> NPs. Obviously, the t-HfO<sub>2</sub> seeds promoted the growth of t-HfO<sub>2</sub> and inhibited the formation of m-HfO<sub>2</sub>. This is a strong evidence for the fact that the growth and phase transformation of t-HfO<sub>2</sub> NPs follow the non-aggregation and surface-deposition growth model.<sup>23,29</sup> The seeding technique is undoubtedly useful for preparing the t-HfO<sub>2</sub> NPs, in spite of the difficulty to obtain the t-HfO<sub>2</sub> NPs. Interestingly, in the presence of m-HfO<sub>2</sub> seeds, the main peaks are associated with m-HfO<sub>2</sub>. Due to the addition of monoclinic seeds, the solute monomers deposited on the pre-existing m-HfO<sub>2</sub> seeds, promoting the formation of m-HfO<sub>2</sub> and inhibiting the formation of t-HfO<sub>2</sub>. In

a word, the product was t-HfO<sub>2</sub> in the presence of t-HfO<sub>2</sub> seeds, and that was m-HfO<sub>2</sub> in the presence of m-HfO<sub>2</sub> seeds. That means, crystal form of seeds determines that of the product. It is a very interesting and significant result, as the saying goes “You must reap what you have sown”.

### Formation mechanisms of HfO<sub>2</sub> by a hydrothermal route

**Formation of m-HfO<sub>2</sub> NPs from t-HfO<sub>2</sub> NPs.** Three cell types of HfO<sub>2</sub> forms are monoclinic (M), tetragonal (T) and cubic (C) as shown in Fig. 10. The coordination numbers of Hf<sup>4+</sup> both in cubic and tetragonal cells are 8 to form Hf-O<sub>8</sub><sup>2-</sup> structure, while that of monoclinic cell is 7 to form Hf-O<sub>7</sub><sup>2-</sup> structure. The structure of m-HfO<sub>2</sub> can be viewed that the t-HfO<sub>2</sub> deflects a certain angle, along the β axis. Usually, structures with coordination number of 8 have better geometric symmetry and are easier to form, but monoclinic cell with coordination number of 7 is stable thermodynamically indeed. Under normal temperatures, the m-HfO<sub>2</sub> is the most stable, which is a reason for obtaining t-HfO<sub>2</sub> NPs with difficulty.

In terms of structures of t-HfO<sub>2</sub> and m-HfO<sub>2</sub>, t-HfO<sub>2</sub> has better geometric symmetry compared with m-HfO<sub>2</sub>, and a rule of thumb is that better symmetry products usually have good kinetic stability and are easy to be produced preferentially. Generally, the occurrence of any reaction or variance is comprehensively selected or controlled by both factors of thermodynamics and kinetics, and the reaction in the initial stage is controlled mainly by factor of kinetics.

In our experiment, t-HfO<sub>2</sub> NPs are easier to form compared with m-HfO<sub>2</sub> NPs and then the t-HfO<sub>2</sub> gradually transforms to m-HfO<sub>2</sub> with temperature rising or time going. In our previous work,<sup>28</sup> the m-HfO<sub>2</sub> NPs were obtained at 160 °C with 3.0 M NaOH for 24 h, but in the early stage of this reaction (1 h and 3 h), the products were t-HfO<sub>2</sub> NPs. It can be deduced that generally t-HfO<sub>2</sub> is produced originally and m-HfO<sub>2</sub> will be

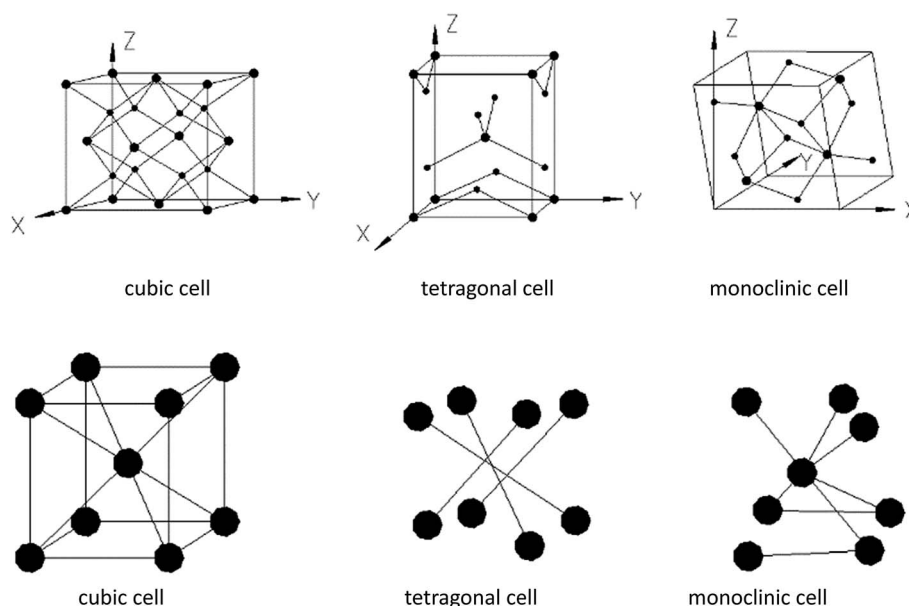


Fig. 10 Structures of different HfO<sub>2</sub> crystal cells.



obtained by transformation from t-HfO<sub>2</sub>. We have mentioned that under adequate temperature and concentration of NaOH, the products were a mixture of t-HfO<sub>2</sub> and m-HfO<sub>2</sub>. Moreover, based on the influence of temperature and concentration of NaOH on products, it is confirmed that t-HfO<sub>2</sub> is produced originally and m-HfO<sub>2</sub> is obtained by transformation from t-HfO<sub>2</sub>. Therefore, it can be concluded that t-HfO<sub>2</sub> is stable kinetically and m-HfO<sub>2</sub> is stable thermodynamically.

To further confirm it above, the aging time of the reaction at 100 °C with 3.0 M NaOH was extended from 24 h to 168 h, the XRD spectra are shown in Fig. 11. Obviously, the products were mainly t-HfO<sub>2</sub> NPs after 24 h, but after 168 h, the products were mainly m-HfO<sub>2</sub> NPs. Passage of time led to the weakening of peaks of t-HfO<sub>2</sub> and the appearance of the peaks of m-HfO<sub>2</sub> in Fig. 11. After 168 h, it was surprising to see that all of t-HfO<sub>2</sub> NPs was transformed to m-HfO<sub>2</sub> NPs. The result offers a clear proof that the m-HfO<sub>2</sub> is stable thermodynamically and the m-HfO<sub>2</sub> is commonly transformed from t-HfO<sub>2</sub>.

The formation of t-HfO<sub>2</sub> with high geometric symmetry becomes more possible in alkaline circumstance. Contrarily, the formation of m-HfO<sub>2</sub> is probably inhibited when the concentration of NaOH in solution is enough high. It is reasonable that high concentration of NaOH can inhibit transformation from t-HfO<sub>2</sub> to m-HfO<sub>2</sub>, because high concentration of NaOH can offer more coordinating oxygen ions and then more oxygen ions are beneficial for formation of oxides with high coordination number. These oxygen ions increase the possibility of the occurrence of the structure with high coordination number and high symmetry, and reduce that of the occurrence of distortion, leading to the formation of t-HfO<sub>2</sub> NPs. In a word, high concentration of NaOH is beneficial for formation of t-HfO<sub>2</sub> and inhibits the formation of m-HfO<sub>2</sub>, this has been confirmed by our previous report.<sup>28</sup> More interestingly, it is also found that with the increased concentration of NaOH, the size of the obtained t-HfO<sub>2</sub> decreased in the concentrated NaOH aqueous solution.

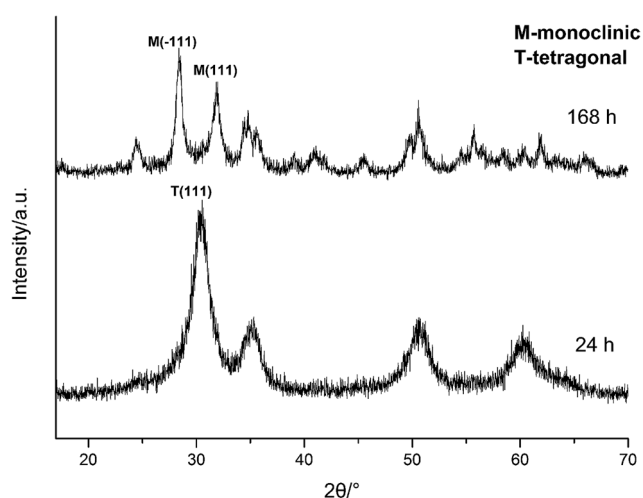


Fig. 11 XRD spectra of HfO<sub>2</sub> NPs prepared under otherwise the standard conditions (3.0 M NaOH and 100 °C) with different reaction time.

On the other hand, temperature is often an important factor to determine the reaction direction and even to determine the crystal form of products. In this work, it has been found that the high temperature is beneficial for the formation of m-HfO<sub>2</sub>. It could be caused by particles annealing and the difference in the structures of the two forms of HfO<sub>2</sub>. Generally, large crystals can be formed by annealing of small crystals, along with the change in the crystal forms in some cases. Therefore, with the rise in temperature, the transformation of t-HfO<sub>2</sub> to m-HfO<sub>2</sub> can be explained in terms of the collision and the distortion in the process of the annealing. It has been reported that with the increase of temperature, the particles are more likely to collide, resulting in the reduction of coordination number, thus forming a large particle.<sup>23–25</sup> As a result, these small t-HfO<sub>2</sub> crystals were transformed to large m-HfO<sub>2</sub> crystals due to the reduction of coordination number.

#### Formation process of HfO<sub>2</sub> NPs with and without seeds.

Generally, the meta-stable t-HfO<sub>2</sub> NPs are formed firstly due to their high formation rate. Then, with the passage of time, the particles change from t-HfO<sub>2</sub> to m-HfO<sub>2</sub> with thermodynamic stability. Based on the significant analyses in the former parts, the formation process of HfO<sub>2</sub> by the hydrothermal route is illustrated as follows.

In Fig. 12, after accomplishment of reaction between hafnium hydroxide chlorides and OH<sup>-</sup> in the water, the precursory complex Hf(OH)<sub>x</sub><sup>4-x</sup> (x ≥ 5) gather and react in the water. Through nucleation of solute monomers without seeds, the meta-stable t-HfO<sub>2</sub> NPs appear. Under appropriate conditions, the product is a mixture of t-HfO<sub>2</sub> NPs and m-HfO<sub>2</sub> NPs because some t-HfO<sub>2</sub> NPs transform to m-HfO<sub>2</sub> NPs. However, the main product is m-HfO<sub>2</sub> NPs under higher temperature and lower alkali, whereas the product under the opposite conditions is t-HfO<sub>2</sub> NPs. In other words, higher temperature and lower alkali concentration are beneficial for the formation of m-HfO<sub>2</sub>. For better control of crystal forms, the seeds are added. When the adequate t-HfO<sub>2</sub> seeds exist, the solute monomers will deposit on t-HfO<sub>2</sub> seeds and the size of formed t-HfO<sub>2</sub> NPs become larger and larger, inhibiting aggregation and the formation of secondary particles, and then preventing the production of m-HfO<sub>2</sub> NPs. Obviously, the t-HfO<sub>2</sub> seeds promote the growth of t-HfO<sub>2</sub> and inhibit the formation of m-HfO<sub>2</sub>. In the other hand, when the m-HfO<sub>2</sub> seeds are added, the solute monomers will deposit on the pre-existing m-HfO<sub>2</sub> seeds, promoting the formation of m-HfO<sub>2</sub> and inhibiting the formation of t-HfO<sub>2</sub>. In a word, the product is t-HfO<sub>2</sub> in the presence of t-HfO<sub>2</sub> seeds, and that is m-HfO<sub>2</sub> in the presence of m-HfO<sub>2</sub> seeds.

For nucleation, the overall Gibbs free energy change,<sup>30</sup> ΔG, should be considered. ΔG, is the sum of the free energy due to the formation of the cluster and that due to the new surface created. In Fig. 13(b), ΔG has a positive maximum at a critical size, r\*. This maximum free energy change is the activation energy for nucleation. Nuclei or clusters larger than the critical size will further decrease their free energy for growth and become stable ones that grow to form particles.

Usually, it is somewhat hard to make ΔG < 0 in the absence of seeds. However, once the seeds preformed stably are added,





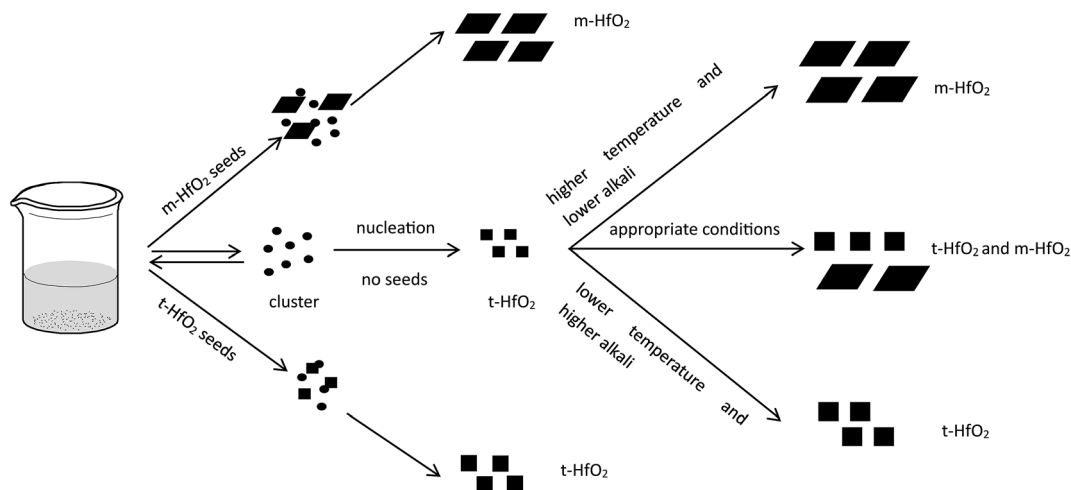


Fig. 12 Formation and transformation processes of  $\text{HfO}_2$  NPs with and without seeds.

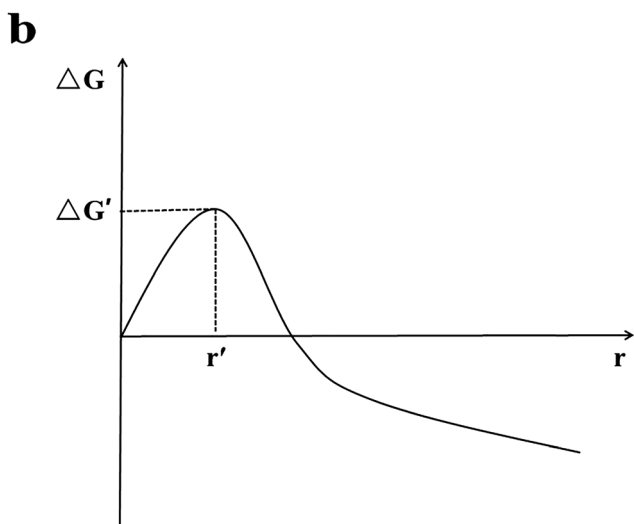
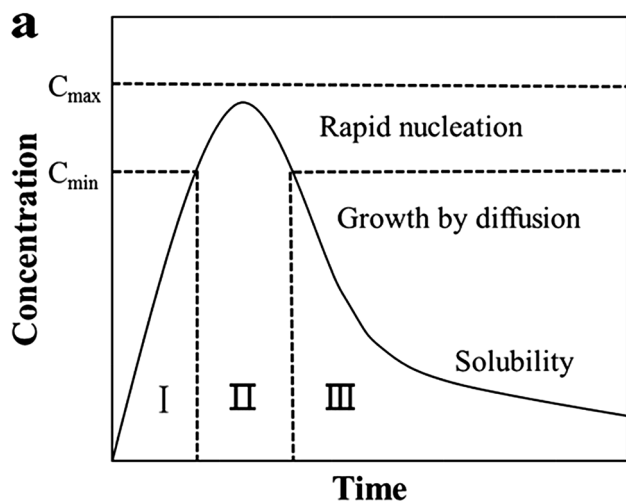


Fig. 13 (a) LaMer model schematic diagram<sup>32</sup> and (b) illustration of the overall free energy  $\Delta G$  as a function of the growth particle size  $r$ .<sup>30</sup>

spontaneous nucleation is inhibited, and then they grow by deposition of monomers on their surfaces to become large particles. At this time, the overall free energy change  $\Delta G$ , could be much lowered even to less than 0. That means, the formation process of stable solute clusters or particles is skipped (Fig. 13(a)) and the reaction is accelerated. Therefore, the resulting final nanoparticles are smaller in size and more evenly dispersed. Undoubtedly, the seeding technique is useful for the systematic control of crystal form and for the study of the growth and nucleation mechanisms.<sup>31</sup>

**Reaction and precursor species for formation of  $\text{HfO}_2$  NPs.** Generally, in aqueous solution, pH affects the concentration of hydro-complexes. By analysis and calculation of the equilibrium constants involving hydrolysis of hafnium ions from D. Rai's report,<sup>33</sup> the changes of mole fractions of the four main hydro-complex species with pH are summarized and shown in Fig. 14. In our work, we measured the yield of t- $\text{HfO}_2$  NPs under different pH. These t- $\text{HfO}_2$  NPs were prepared at 100 °C

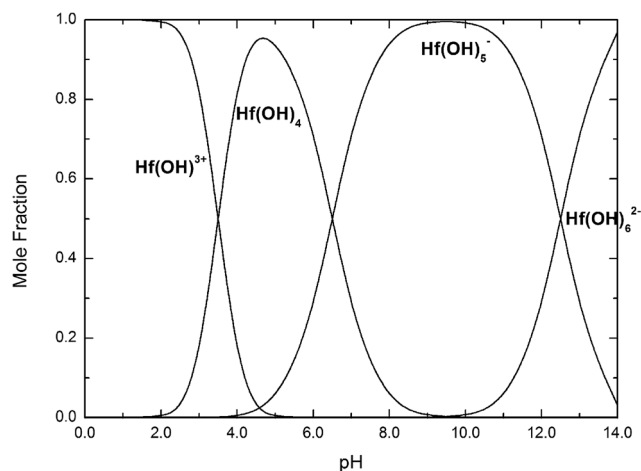
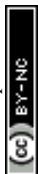


Fig. 14 Mole fractions of  $\text{Hf}(\text{OH})^{3+}$ ,  $\text{Hf}(\text{OH})_4$ ,  $\text{Hf}(\text{OH})_5^-$ ,  $\text{Hf}(\text{OH})_6^{2-}$  complexes as a function of pH at 25 °C.





nanoparticles. In the presence of seeds, the declined activated energy for the reaction is due to the decrease of  $\Delta G$ , resulting from the skipping of spontaneous nucleation stage, and then causing separation of nucleation from growth.

The effect of solution pH on the formation of HfO<sub>2</sub> NPs was learned by the analysis above. Meantime, the high concentration of NaOH promoted the formation of t-HfO<sub>2</sub> NPs. Therefore, the hydro-complex Hf(OH)<sub>6</sub><sup>2-</sup> has been confirmed as the precursor complex to form HfO<sub>2</sub> particles.

## Acknowledgements

The authors gratefully acknowledge the Foundation of Shanghai Municipal Commission of Economy and Informatization (15XI-1-28).

## Notes and references

- 1 C. A. Mirkin, R. L. Letsinger, R. C. Mucic and J. J. Storhoff, *Nature*, 1996, **382**, 607–609.
- 2 D. L. Feldheim and C. D. Keating, *Chem. Soc. Rev.*, 1998, **27**, 1–12.
- 3 S. Saito, *Science*, 1997, **278**, 77–78.
- 4 J. Robertson, *Rep. Prog. Phys.*, 2006, **69**, 327–396.
- 5 J. De Roo, K. De Keukeleere, J. Feys, P. Lommens, Z. Hens and I. Van Driessche, *J. Nanopart. Res.*, 2013, **15**, 1778.
- 6 G. D. Wilk, R. M. Wallace and J. M. Anthony, *J. Appl. Phys.*, 2001, **89**, 5243–5275.
- 7 J. Molina, R. Ortega, W. Calleja, P. Rosales, C. Zuniga and A. Torres, *Mater. Sci. Eng., B*, 2012, **177**, 1501–1508.
- 8 S. A. Eliziario, L. S. Cavalcante, J. C. Sczancoski, P. S. Pizani, J. A. Varela, J. W. M. Espinosa and E. Longo, *Nanoscale Res. Lett.*, 2009, **4**, 1371–1379.
- 9 R. Terki, G. Bertrand, H. Aourag and C. Coddet, *Mater. Lett.*, 2008, **62**, 1484–1486.
- 10 V. Jayaraman, G. Bhavesh, S. Chinnathambi, S. Ganesan and P. Aruna, *Mater. Express*, 2014, **4**, 375–383.
- 11 W. E. Buhro and V. L. Colvin, *Nat. Mater.*, 2003, **2**, 138–139.
- 12 H. B. Yao, M. R. Gao and S. H. Yu, *Nanoscale*, 2010, **2**, 323–334.
- 13 E. Tirosh and G. Markovich, *Adv. Mater.*, 2007, **19**, 2608–2612.
- 14 J. S. Quintero-Garcia, B. A. Puente-Urbina, L. A. Garcia-Cerda, O. S. Rodriguez-Fernandez and E. Mendoza-Mendoza, *Mater. Lett.*, 2015, **159**, 520–524.
- 15 A. Ramadoss, K. Krishnamoorthy and S. J. Kim, *Mater. Lett.*, 2012, **75**, 215–217.
- 16 A. Sahraneshin, S. Asahina, T. Togashi, V. Singh, S. Takami, D. Hojo, T. Arita, K. Minami and T. Adschiri, *Cryst. Growth Des.*, 2012, **12**, 5219–5226.
- 17 P. E. Meskin, F. Y. Sharikov, V. K. Ivanov, B. R. Churagulov and Y. D. Tretyakov, *Mater. Chem. Phys.*, 2007, **104**, 439–443.
- 18 E. Montes, P. Ceron, T. R. Montalvo, J. Guzman, M. Garcia-Hipolito, A. B. Soto-Guzman, R. Garcia-Salcedo and C. Falcony, *Appl. Radiat. Isot.*, 2014, **83**, 196–199.
- 19 L. Xiang, Y. P. Yin and Y. Jin, *J. Mater. Sci.*, 2002, **37**, 349–352.
- 20 H. B. Yin, Y. Wada, T. Kitamura, S. Kambe, S. Murasawa, H. Mori, T. Sakata and S. Yanagida, *J. Mater. Chem.*, 2001, **11**, 1694–1703.
- 21 Y. Q. Zheng, E. R. Shi, Z. Z. Chen, W. J. Li and X. F. Hu, *J. Mater. Chem.*, 2001, **11**, 1547–1551.
- 22 T. T. Shi, Y. T. Cai, L. Liu and X. P. Zhou, *Colloids Surf., A*, 2015, **469**, 83–92.
- 23 T. Sugimoto, X. P. Zhou and A. Muramatsu, *J. Colloid Interface Sci.*, 2003, **259**, 43–52.
- 24 T. Sugimoto, X. P. Zhou and A. Muramatsu, *J. Colloid Interface Sci.*, 2002, **252**, 339–346.
- 25 T. Sugimoto and X. P. Zhou, *J. Colloid Interface Sci.*, 2002, **252**, 347–353.
- 26 L. Liu, J. C. Xue and X. P. Zhou, *Nanosci. Nanotechnol. Lett.*, 2014, **6**, 346–352.
- 27 C. Jia, Y. Cheng, F. Bao, D. Chen and Y. Wang, *J. Cryst. Growth*, 2006, **294**, 353–357.
- 28 J. J. Qi and X. P. Zhou, *Colloids Surf., A*, 2015, **487**, 26–34.
- 29 X. P. Zhou, S. S. Li, X. L. Chen, Q. Zhu, Z. Q. Wang and J. Zhang, *J. Nanosci. Nanotechnol.*, 2008, **8**, 1392–1397.
- 30 I. V. Markov, *Crystal growth for beginners: fundamentals of nucleation, crystal growth and epitaxy*, World Scientific, 2003.
- 31 S. Taotao, C. Yutian, L. Li and Z. Xingping, *Colloids Surf., A*, 2015, **469**, 83–92.
- 32 C. Burda, X. Chen, R. Narayanan and M. A. El-Sayed, *Chem. Rev.*, 2005, **105**, 1025–1102.
- 33 D. Rai, Y. X. Xia, N. J. Hess, D. M. Strachan and B. P. McGrail, *J. Solution Chem.*, 2001, **30**, 949–967.
- 34 X. S. Zheng, L. Liu and X. P. Zhou, *Colloid J.*, 2014, **76**, 558–563.
- 35 R. R. Piticescu, C. Monty, D. Taloi, A. Motoc and S. Axinte, *J. Eur. Ceram. Soc.*, 2001, **21**, 2057–2060.

